Electronic Supporting Information (ESI)

Potassium Supporting Electrolyte Enhances Stability of Ti-substituted Polyoxovanadates for Nonaqueous Redox Flow Batteries

*Mamta Dagar, William W. Brennessel, and Ellen M. Matson**

Department of Chemistry, University of Rochester, Rochester, NY 14627, USA

Email: matson@chem.rochester.edu

Supporting Information Table of Contents

Experimental methods:

Determining D_0. 5 mM concentration of the cluster $[Ti_2V_4O_5(OMe)_{14}]$, with 0.1 M KPF_6 as the supporting electrolyte were used in acetonitrile. CV measurements were carried out inside a nitrogen filled glove box (MBraun, USA) using a Bio-Logic SP 150 potentiostat/galvanostat and the EC-Lab software suite. Cyclic voltammograms were recorded using a 3 mm diameter glassy carbon working electrode (CH Instruments, USA), a Pt wire auxiliary electrode (CH Instruments, USA), and a Ag/Ag^+ non-aqueous reference electrode with 0.01 M $AgNO_3$ in 0.1 M $[^nBu_4N][PF_6]$in CH_3CN (Bio-Logic). Cyclic voltammograms were *iR* compensated at 95% with impedance taken at 100 kHz using the ZIR tool included within the EC-Lab software.

The diffusion coefficient associated with each redox couple was determined by using the slope of the peak current (i_p) versus the square root of scan rate $v^{1/2}$. The Randles – Sevcik equation was used to estimate the diffusion coefficients from CV data. For a reversible redox couple, the peak current is given by the Eqn S1:

$$i_p = 2.69 \times 10^5 \, n^{3/2} \, A \, c \, D_0^{1/2} \, v^{1/2} \qquad \text{Eqn S1}$$

In eq. S1, *n* is the number of electrons transferred; *A* is the electrode area (0.0707 cm^2 for the glassy carbon working electrode); *c* is the bulk concentration of the active species; D_0 is the diffusion coefficient of the active species; v is the scan rate. For an irreversible redox couple, the peak current, is given by the Eqn S2:

$$i_p = 2.99 \times 10^5 \, n^{3/2} \, \alpha^{1/2} A \, c \, D_0^{1/2} \, v^{1/2} \qquad \text{Eqn S2}$$

where α is the charge transfer coefficient. For this study, α = 0.5.

For the redox couples that show quasi-reversible kinetics, relationships for both reversible and irreversible redox reaction are usually employed to determine the diffusion coefficients of such redox processes. Therefore, an average value of diffusion coefficient was approximated for a quasi-reversible redox couple using both equations S1 and S2.[1-3]

Calculation of k_0. The electron-transfer kinetics was estimated directly from CV measurements by using the Nicholson method.[4] The potential difference (ΔEp) of oxidation and reduction peaks were obtained at different scan rates. The transfer parameter, ψ, was extracted from the working curve constructed by Nicholson using ΔEp values. The standard heterogeneous charge-transfer rate constant, k_0, for a given electron transfer process was determined using Eqn S3:

$$\Psi = \nu^{-1/2} k_0 \left({}^{\pi n F D_0}/_{RT} \right)^{-1/2} \qquad \text{Eqn S3}$$

where n is the number of electrons transferred, F is the Faraday constant, D is the diffusion coefficient, v is the scan rate, R is the ideal gas constant and T is the temperature.

Table S1. Substoichiometric electrochemical titration of $LiPF_6$ into $[Ti_2V_4O_5(OMe)_{14}]$ analyzed by SWV.

Equivalents of $LiPF_6$ added	$E_{1/2}$ (V)	
	2^{nd} Ti^{III}/Ti^{IV} couple	1^{st} Ti^{III}/Ti^{IV} couple
0 eq.	-2.09 V	-1.60 V
0.2 eq.	-2.08 V	-1.60 V
0.4 eq.	-2.08 V	-1.59 V
0.6 eq.	-2.03 V	-1.58 V
0.8 eq.	-2.02 V	-1.58 V
1 eq.	-2.01 V	-1.57 V
1.2 eq.	-2.00 V	-1.55 V
2 eq.	-	-1.52 V

Table S2. Substoichiometric electrochemical titration of LiOTf into $[Ti_2V_4O_5(OMe)_{14}]$ analyzed by SWV.

Equivalents of LiOTf added	$E_{1/2}$ (V)	
	2^{nd} Ti^{III}/Ti^{IV} couple	1^{st} Ti^{III}/Ti^{IV} couple
0 eq.	-2.09 V	-1.60 V
0.2 eq.	-2.02 V	-1.59 V
0.4 eq.	-1.99 V	-1.59 V
0.6 eq.	-2.00 V	-1.58 V
0.8 eq.	-1.98 V	-1.57 V
1 eq.	-1.98 V	-1.56 V
1.2 eq.	-1.98 V	-1.56 V
2 eq.	-	-1.50 V

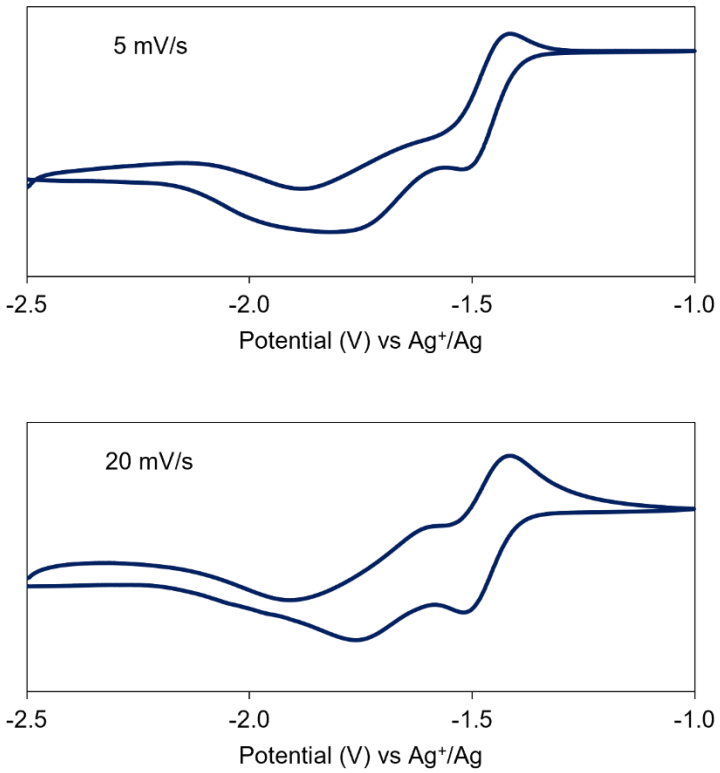

Figure S1. CVs of reduction events of $[Ti_2V_4O_5(OMe)_{14}]$ with 0.1 M $LiPF_6$ in acetonitrile at 5 mV/s (top) and 20 mV/s (bottom).

Table S3. Substoichiometric electrochemical titration of KPF_6 into $[Ti_2V_4O_5(OMe)_{14}]$ analyzed by SWV.

Equivalents of KPF_6 added	$E_{1/2}$ (V)	
	2^{nd} Ti^{III}/Ti^{IV} couple	1^{st} Ti^{III}/Ti^{IV} couple
0 eq.	-2.10 V	-1.60 V
0.2 eq.	-2.04 V	-1.60 V
0.4 eq.	-2.04 V	-1.60 V
0.6 eq.	-2.04 V	-1.59 V
0.8 eq.	-2.03 V	-1.59 V
1 eq.	-2.03 V	-1.59 V
1.2 eq.	-2.01 V	-1.59 V
2 eq.	-2.01 V	-1.59 V

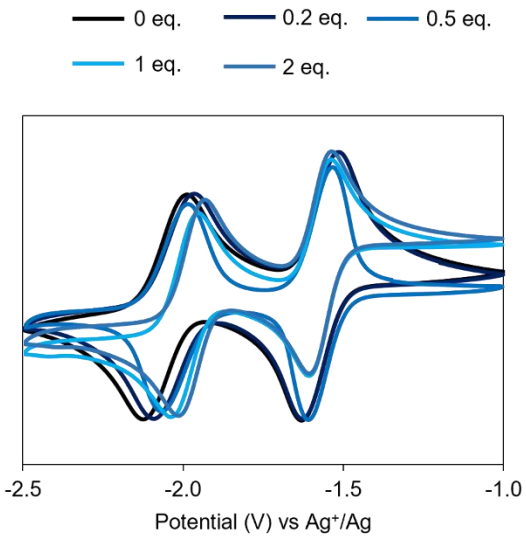

Figure S2. CVs of titration experiments conducted with substoichiometric titrations of KPF_6 into 5mM $[Ti_2V_4O_5(OMe)_{14}]$ solution in acetonitrile with 0.1 M $TBAPF_6$.

Table S4. DMF titration in the $[Ti_2V_4O_5(OMe)_{14}]$ solution originally with 0.1 M $TBAPF_6$ that is pre-titrated with KPF_6.

Volume of DMF added	$E_{1/2}$ (V)	
	2^{nd} Ti^{III}/Ti^{IV} couple	1^{st} Ti^{III}/Ti^{IV} couple
0 µL	-1.94 V	-1.57 V
50 µL	-1.94 V	-1.57 V
100 µL	-1.94 V	-1.57 V
200 µL	-1.99 V	-1.57 V
400 µL	-2.00 V	-1.57 V
500 µL	-2.00 V	-1.57 V
700 µL	-2.01 V	-1.57 V
1 mL	-2.03 V	-1.57 V
2 mL	-2.06 V	-1.57 V
4 mL	-2.10 V	-1.58 V

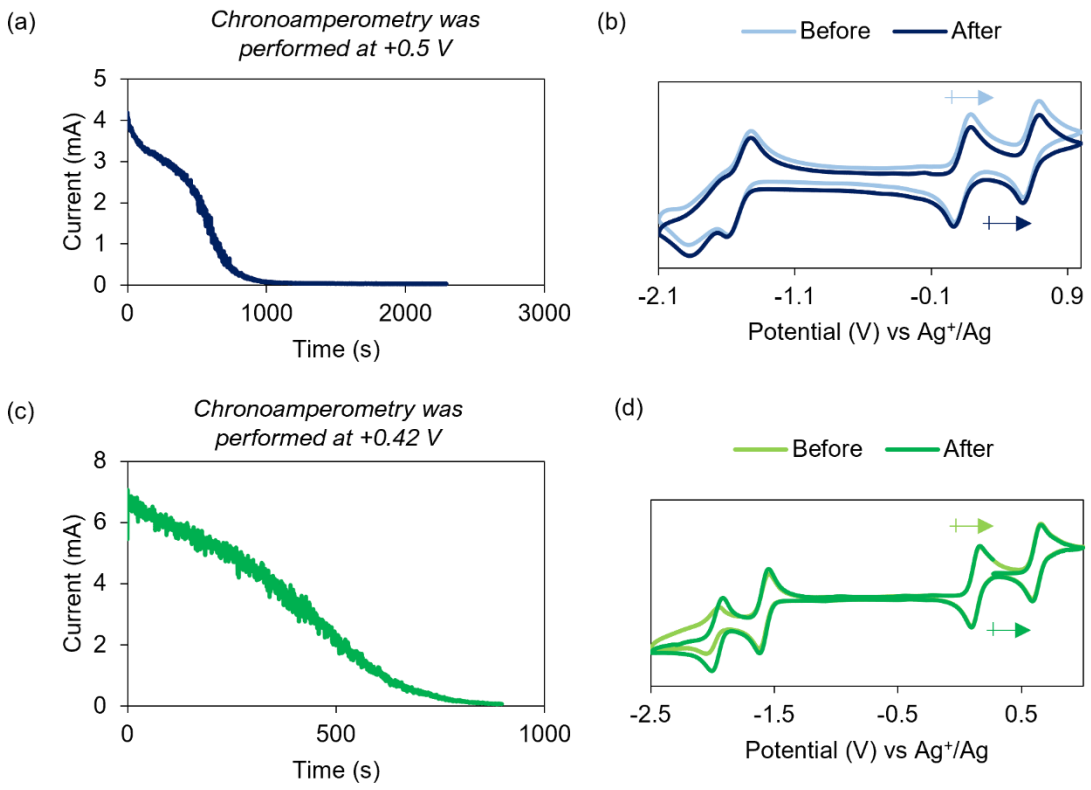

Figure S3. Bulk oxidation of $[Ti_2V_4O_5(OMe)_{14}]$ in $LiPF_6$ (top, blue) and KPF_6 (bottom, green). (a) and (c) represent the corresponding *I-t* curves. (b) and (d) denote the CVs before and after chronoamperometry measurements. The arrows denote the open circuit voltage associated with each CV trace.

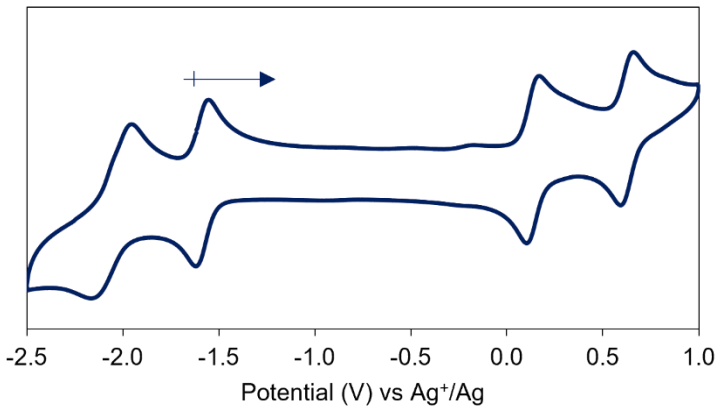

Figure S4. Cyclic voltammogram of the synthesized cluster $[K\{Ti_2V_4(OCH_3)_{14}\}]$ recorded at 100 mV/s with 0.1 M $TBAPF_6$ in acetonitrile. The arrow indicates the open circuit voltage of the resultant cluster.

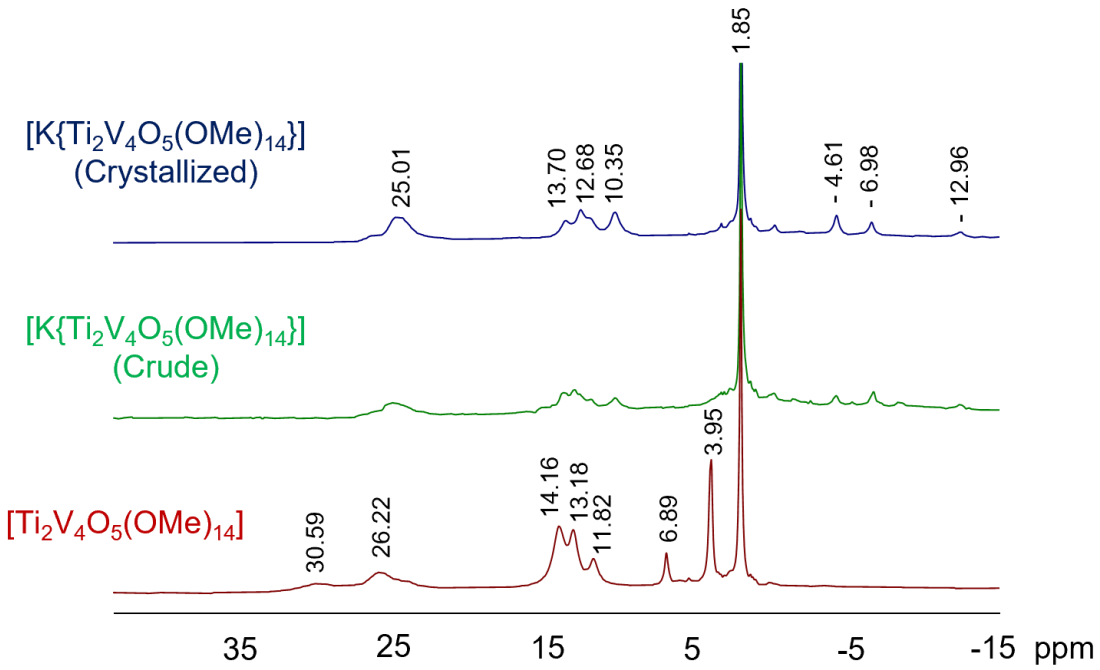

Figure S5. ^{1}H NMR of crude (green) and recrystallized (blue) [K{$Ti_2V_4(OCH_3)_{14}$}] compared to [$Ti_2V_4O_5(OMe)_{14}$] (red). All NMRs are collected in CD_3CN.

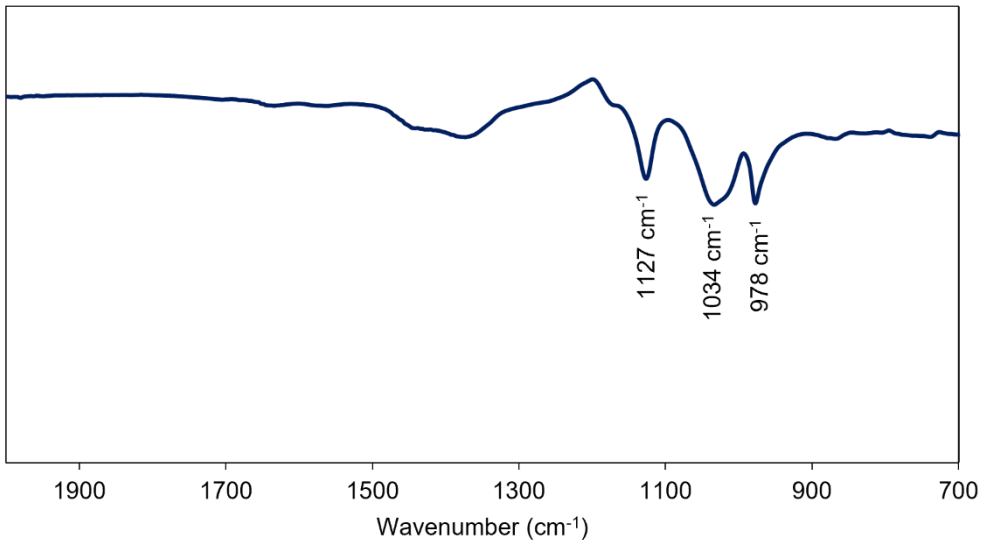

Figure S6. IR spectrum of the synthesized cluster [K{$Ti_2V_4(OCH_3)_{14}$}].

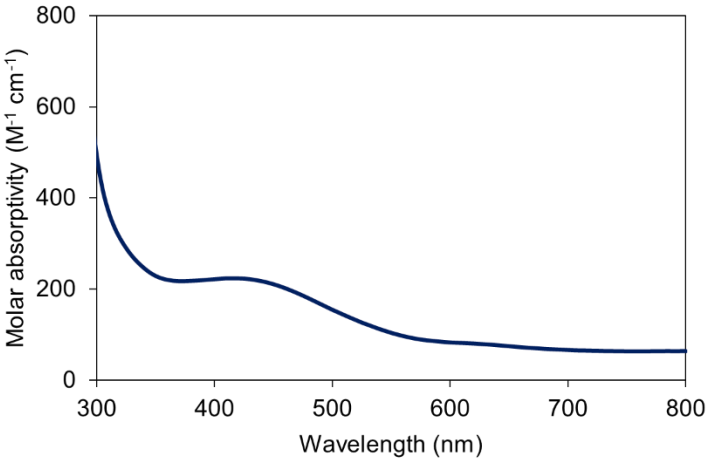

Figure S7. Electronic absorption spectrum of the synthesized cluster [K{$Ti_2V_4(OCH_3)_{14}$}].

Table S5. Crystallographic parameters for molecular structure of **[K{$Ti_2V_4(OCH_3)_{14}$}]**.

Empirical formula	$C_{14}H_{42}KO_{19}Ti_2V_4$
Formula weight	853.13
Temperature	100.01(10) K
Wavelength	1.54184 Å
Crystal system	orthorhombic
Space group	$P2_12_12_1$
Unit cell dimensions	*a* = 8.99550(10) Å α = 90° *b* = 18.26630(10) Å β = 90° *c* = 18.70880(10) Å γ = 90°
Volume	3074.13(4) $Å^3$
Z	4
Reflections collected	38130
Independent reflections	6604 [*R*(int) = 0.0398]
Observed reflections	6418
Completeness to theta = 74.504°	100.0%
Absorption correction	Multi-scan
Max. and min. transmission	1.00000 and 0.38869
Refinement method	Full-matrix least-squares on F^2
Data / restraints / parameters	6604 / 0 / 376
Goodness-of-fit on F^2	1.036
Final *R* indices [*I*>2sigma(*I*)]	*R*1 = 0.0308, *wR*2 = 0.0813
R indices (all data)	*R*1 = 0.0318, *wR*2 = 0.0818
Absolute structure parameter	0.413(7)
Largest diff. peak and hole	1.303 and -0.497 e.$Å^{-3}$

Table S6. Bond valence sum calculations for $K[Ti_2V_4O_5(OMe)_{14}]$ based on X-ray crystallographic data collected at 100 K.

Compound	Ti^{III}	Ti^{IV}	V^{IV}	V^{V}		Bond valence sums					
						Ti(1)	Ti(2)	V(3)	V(4)	V(5)	V(6)
$K[Ti_2V_4O_5(OMe)_{14}]$	1	1	-	-	Ti^{III}	**3.21**	**3.88**	**-**	**-**	**-**	**-**
					Ti^{IV}	**3.43**	**4.01**				
	-	-	4	0	V^{IV}	**-**	**-**	**4.013**	**3.83**	**4.02**	**4.01**
					V^{V}	**-**	**-**	4.22	4.04	4.24	4.22

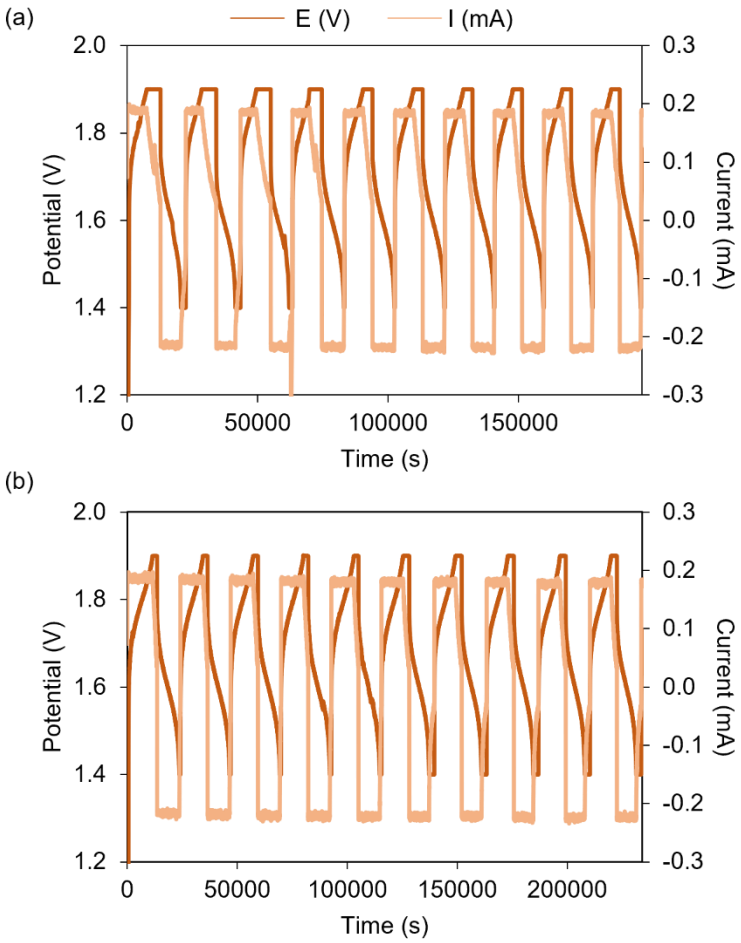

Figure S8. Charge-discharge traces of 10 cycles obtained for $[Ti_2V_4O_5(OMe)_{14}]$ in (a) $TBAPF_6$ (b) KPF_6.

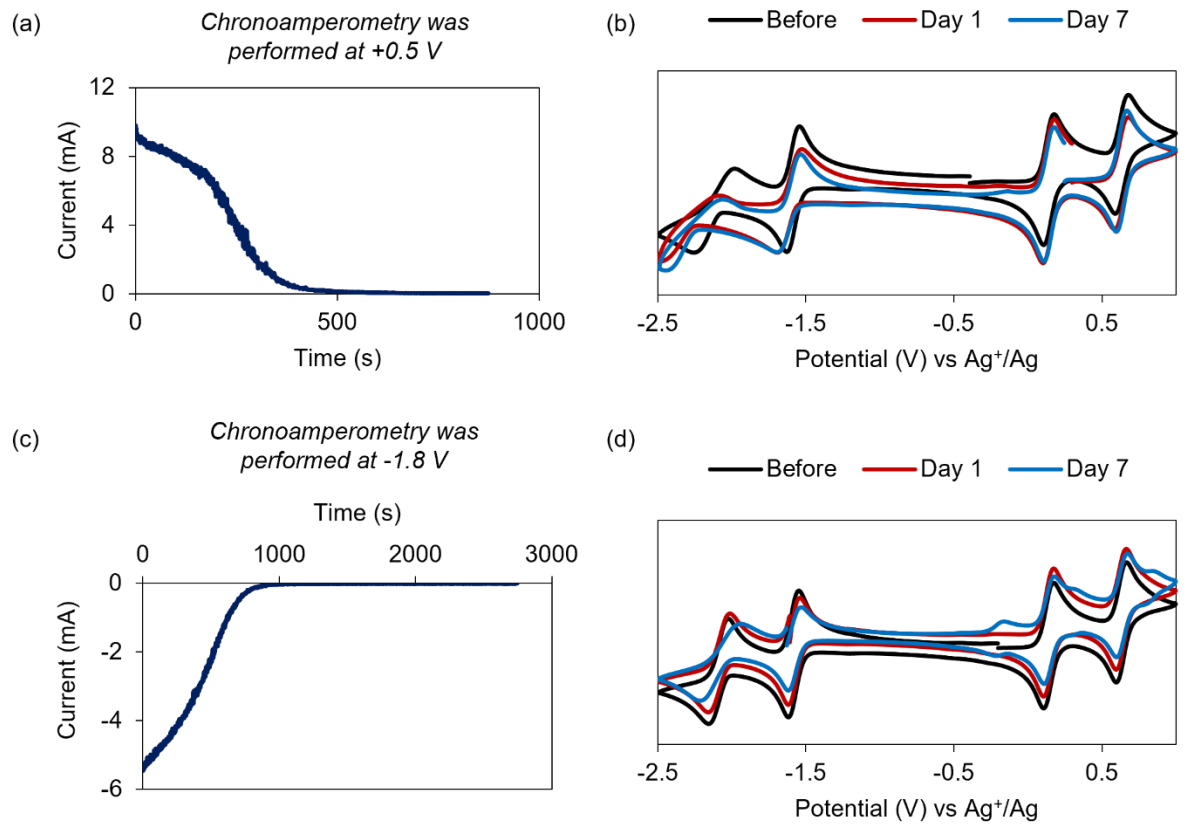

Figure S9. Monitoring of bulk electrolyzed solutions of $[Ti_2V_4O_5(OMe)_{14}]$ in $TBAPF_6$ at 30ºC. (a) and (c) represent *I-t* curves associated with bulk oxidation and bulk reduction, respectively. (b) and (d) represent the corresponding CVs. Bulk electrolysis was carried out at room temperature and the resultant solution was heated at 30ºC for 7 days. Breaks in the voltammograms indicate the open circuit voltage of the resultant solution.

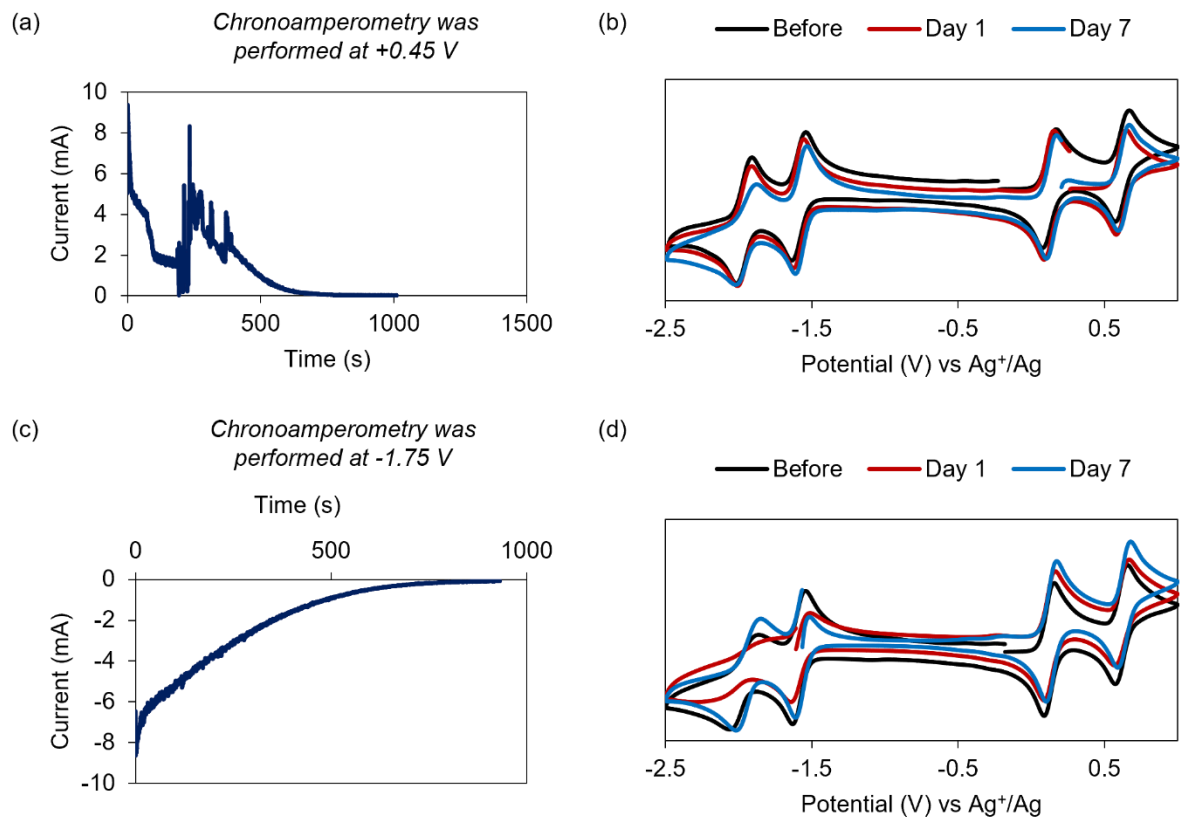

Figure S10. Monitoring of bulk electrolyzed solutions of $[Ti_2V_4O_5(OMe)_{14}]$ in KPF_6 at 30ºC. (a) and (c) represent *I-t* curves associated with bulk oxidation and bulk reduction, respectively. (b) and (d) represent the corresponding CVs. Bulk electrolysis was carried out at room temperature and the resultant solution was heated at 30ºC for 7 days. Breaks in the voltammograms indicate the open circuit voltage of the resultant solution. Note – The spurious responses in (a) are due to the stirring being interrupted during the experiment.

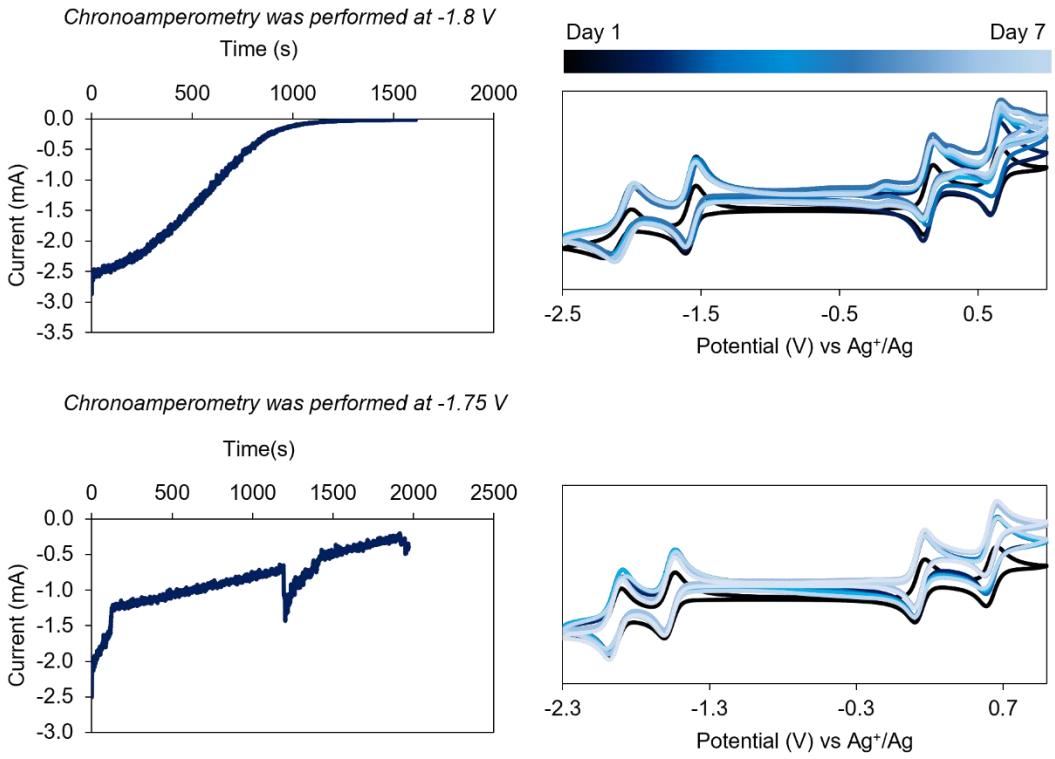

Figure S11. Long-term stability analysis of bulk reduced samples of $[Ti_2V_4O_5(OMe)_{14}]$ in acetonitrile with 0.1 M $[^nBu_4N][PF_6]$ (top) and 0.1 M KPF_6 (bottom) at room temperature.

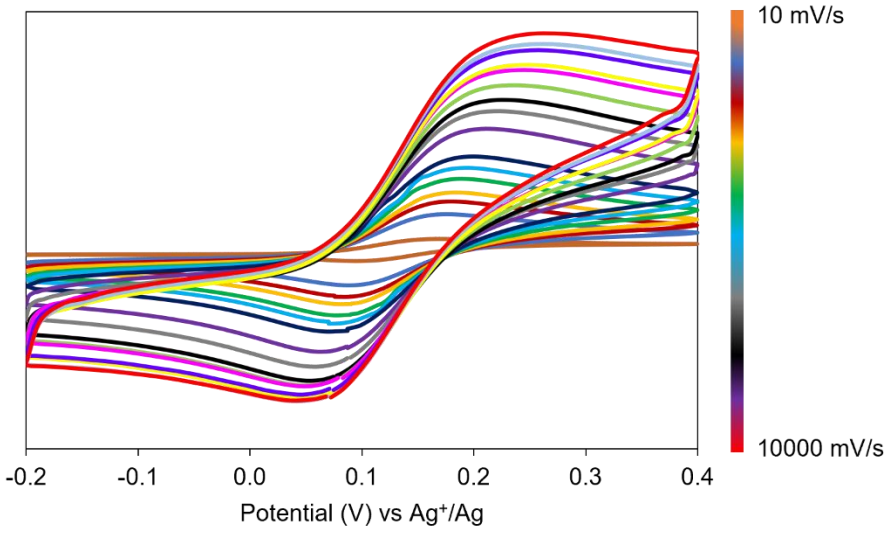

Figure S12. Cyclic voltammograms of $\mathbf{1^+/0}$ redox couple of $[Ti_2V_4O_5(OMe)_{14}]$ with 0.1 M KPF_6 at scan rates ranging from 10 – 10000 mV/s in acetonitrile.

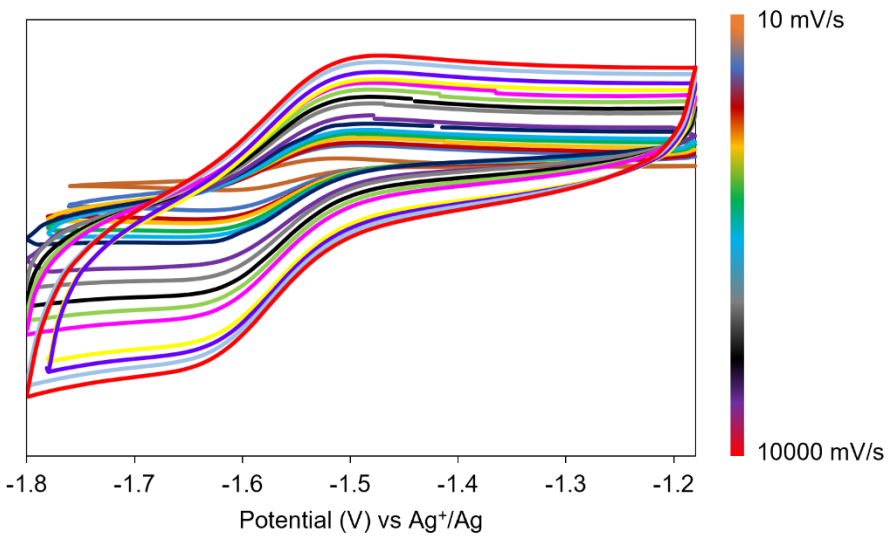

Figure S13. Cyclic voltammograms of **0/1**$^{-}$ redox couple of $[Ti_2V_4O_5(OMe)_{14}]$ with 0.1 M KPF_6 at scan rates ranging from 10 – 10000 mV/s in acetonitrile.

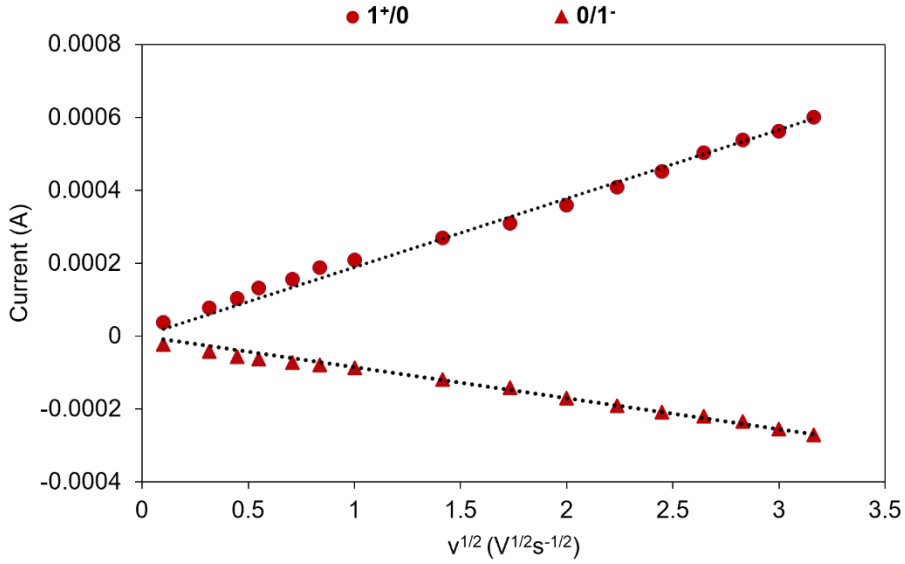

Figure S14. Randles–Sevcik analysis of **1**$^{+}$**/0** and **0/1**$^{-}$ redox couples of $[Ti_2V_4O_5(OMe)_{14}]$ with 0.1 M KPF_6 in acetonitrile.

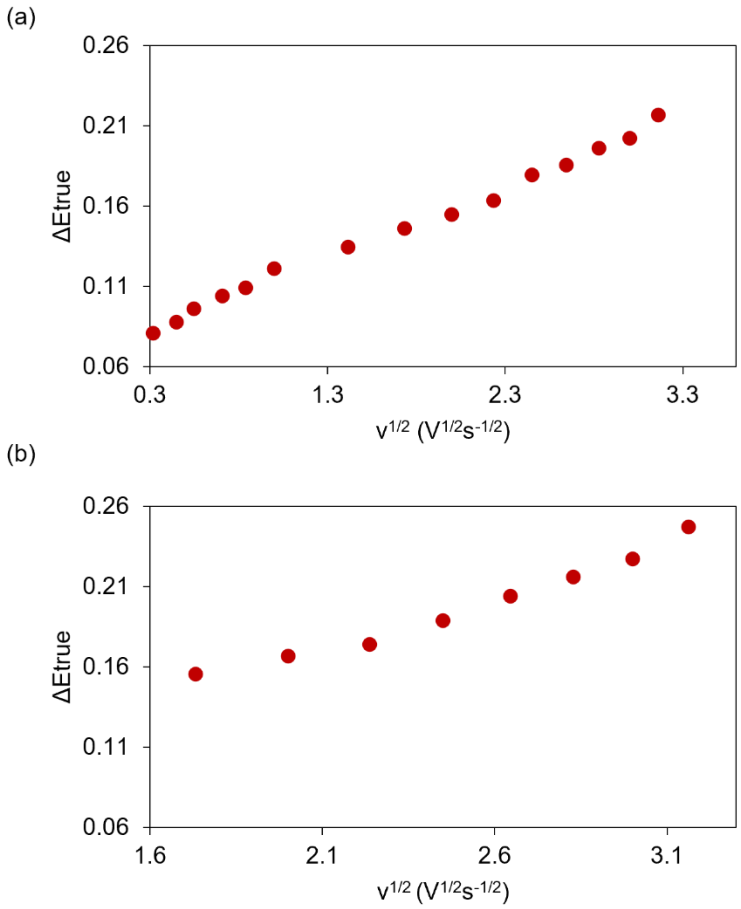

Figure S15. Plot of ΔE_p vs (scan rate)$^{1/2}$ for $[Ti_2V_4O_5(OMe)_{14}]$ with 0.1 M KPF_6 for the (a) **1$^+$/0** and (b) **0/1$^-$** redox couples.

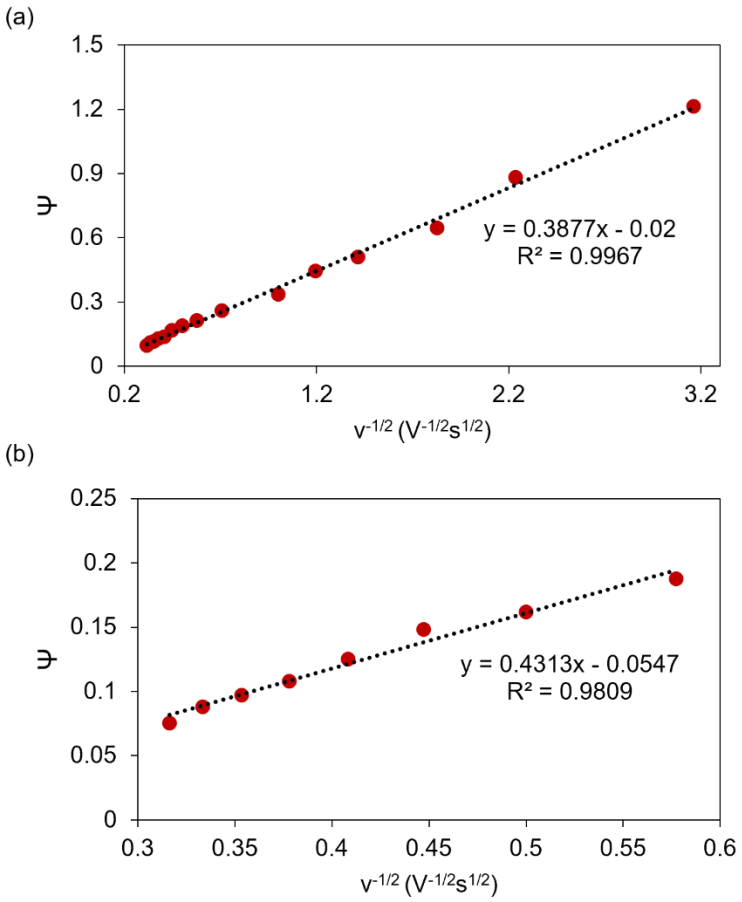

Figure S16. Plot of Ψ vs (scan rate)$^{-1/2}$ for $[Ti_2V_4O_5(OMe)_{14}]$ with 0.1 M KPF_6 for the (a) **1$^+$/0** and (b) **0/1$^-$** redox couples.

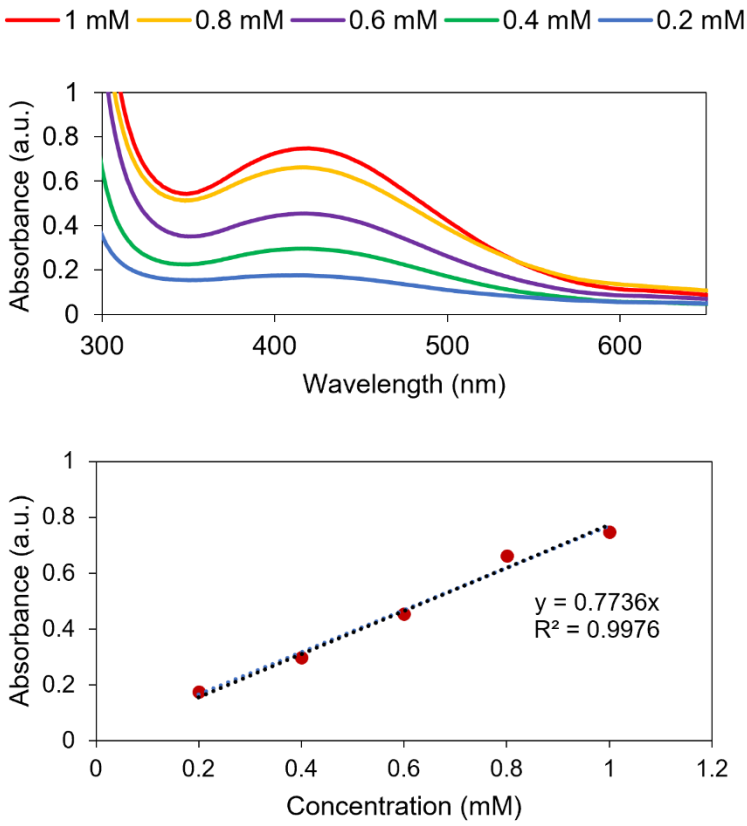

Figure S17. Calibration curve for solubility of $[Ti_2V_4O_5(OMe)_{14}]$ in acetonitrile with 0.1 M KPF_6.

Table S7. Solubility measured for $[Ti_2V_4O_5(OMe)_{14}]$ in acetonitrile with 0.1 M KPF_6.

Trials	Absorbance at 420 nm	Diluted concentration (mM)	Saturated concentration (mM)
1	0.1701	0.2198	43.97
2	0.1727	0.2232	44.64
3	0.1953	0.2524	50.49

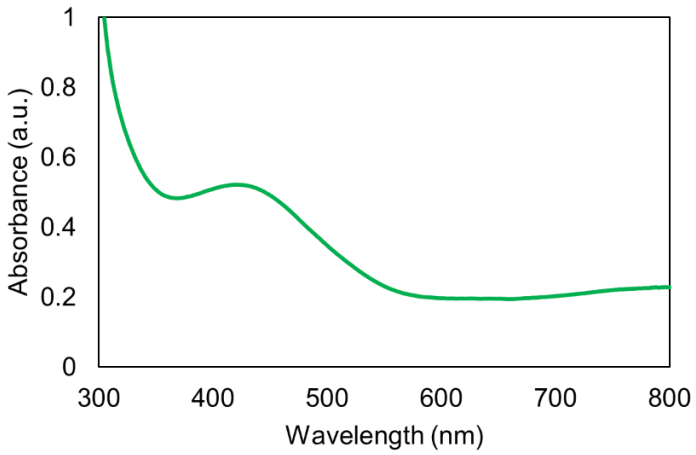

Figure S18. Electronic absorption spectrum of bulk reduced, mono-anionic $[Ti_2V_4O_5(OMe)_{14}]$ in acetonitrile with 0.1 M KPF_6.

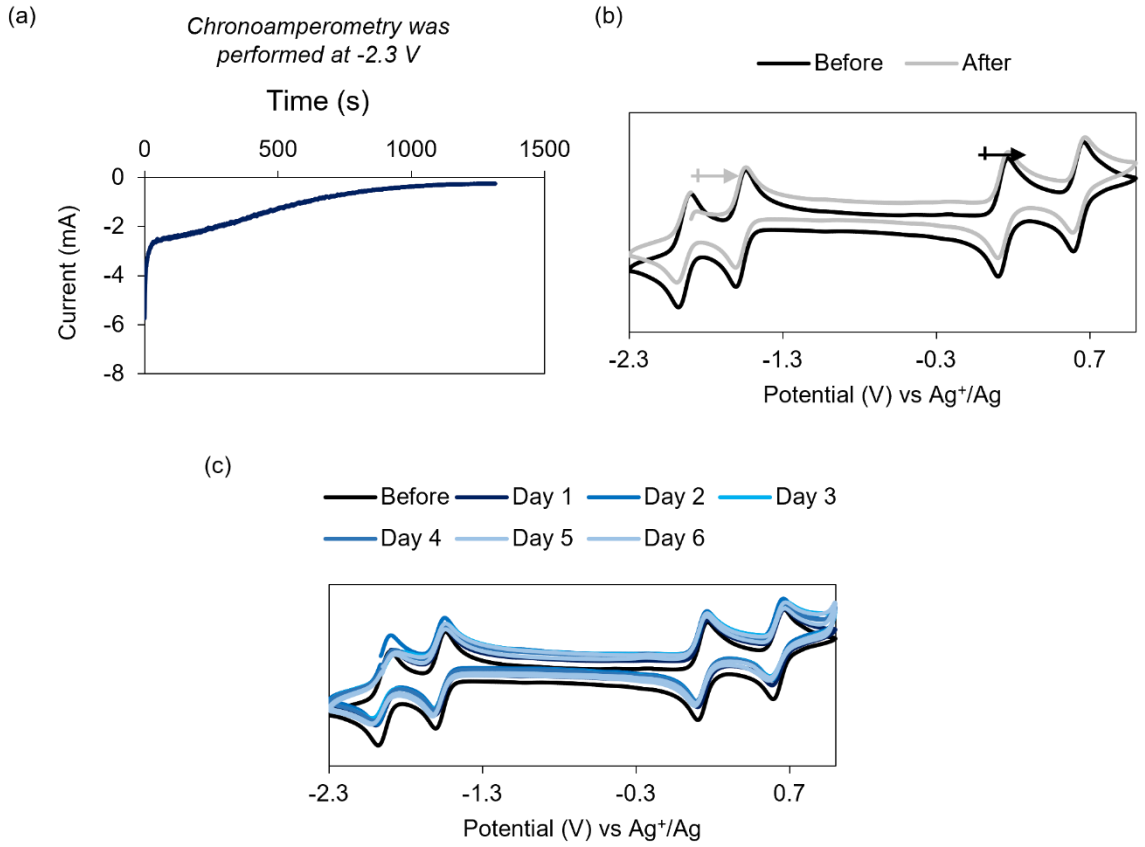

Figure S19. Bulk reduction of $[Ti_2V_4O_5(OMe)_{14}]$ to -2 oxidation state in acetonitrile with 0.1 M KPF_6. (a) represents *I-t* curves associated with bulk reduction (b) depicts the corresponding CVs (c) demonstrates the stability of the bulk reduced sample as monitored via CV at room temperature for 6 days.

References.

1. Liu, Q. H.; Sleightholme, A. E. S.; Shinkle, A. A.; Li, Y. D.; Thompson, L. T. Non-aqueous vanadium acetylacetonate electrolyte for redox flow batteries. *Electrochemistry Communications* **2009**, *11*, 2312-2315.
2. Sleightholme, A. E. S.; Shinkle, A. A.; Liu, Q. H.; Li, Y. D.; Monroe, C. W.; Thompson, L. T. Non-aqueous manganese acetylacetonate electrolyte for redox flow batteries. *Journal of Power Sources* **2011**, *196*, 5742-5745.
3. Kosswattaarachchi, A. M.; VanGelder, L. E.; Nachtigall, O.; Hazelnis, J. P.; Brennessel, W. W.; Matson, E. M.; Cook, T. R. Transport and Electron Transfer Kinetics of Polyoxovanadate-Alkoxide Clusters. *Journal of the Electrochemical Society* **2019**, *166*, A464-A472.
4. Nicholson, R. S. THEORY AND APPLICATION OF CYCLIC VOLTAMMETRY FOR MEASUREMENT OF ELECTRODE REACTION KINETICS. *Analytical Chemistry* **1965**, *37*, 1351-1355.